analytical chemistry

Article

Cite This: *Anal. Chem.* 2019, 91, 13112−13118

pubs.acs.org/ac

Rapid Visualization of Chemically Related Compounds Using Kendrick Mass Defect As a Filter in Mass Spectrometry Imaging

Christopher Kune,[†,∥] Andréa McCann,[†,∥] La Rocca Raphaël,[†] Anthony Arguelles Arias,[‡] Mathieu Tiquet,[†] Daan Van Kruining,[§] Pilar Martinez Martinez,[§] Marc Ongena,[‡] Gauthier Eppe,[†] Loïc Quinton,[†] Johann Far,[†] and Edwin De Pauw*[,†]

[†]Mass Spectrometry Laboratory, MolSys Research Unit, University of Liège, Liège, Belgium

[‡]Microbial Processes and Interactions, Gembloux Agro-Bio Tech, TERRA Teaching and Research Centre, University of Liege, Gembloux, Belgium

[§]Department of Psychiatry and Neuropsychology, School for Mental Health and Neuroscience, Maastricht University, Maastricht, The Netherlands

Supporting Information

ABSTRACT: Kendrick mass defect (KMD) analysis is widely used for helping the detection and identification of chemically related compounds based on exact mass measurements. We report here the use of KMD as a criterion for filtering complex mass spectrometry data set. The method allow automated, easy and efficient data processing, enabling the reconstruction of 2D distributions of families of homologous compounds from MSI images. We show that KMD filtering, based on in-house software, is suitable and robust for high resolution (full width at half-maximum, fwhm, at m/z 410 of 20 000) and very high-resolution (fwhm, at m/z 410 of 160 000) MSI data. This method has been successfully applied to two different types of samples, bacteria cocultures, and brain tissue sections.

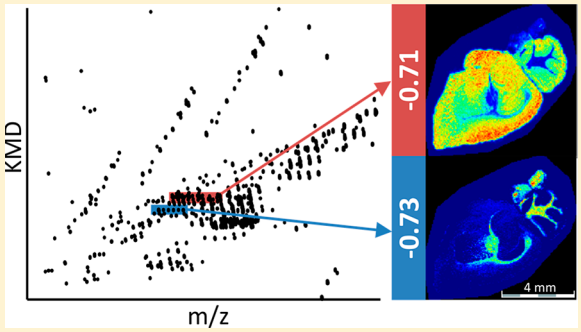

Downloaded via UNIV DE LIEGE on March 4, 2021 at 11:11:15 (UTC).
See https://pubs.acs.org/sharingguidelines for options on how to legitimately share published articles.

Identification of analytes in complex mixtures is still a major challenge in analytical chemistry.[1] For that purpose, mass spectrometers are among the most widely used instruments. They are commonly coupled to direct infusion or hyphenated with separation techniques, for example, liquid chromatography (LC), capillary electrophoresis (CE), ion mobility spectrometry (IMS). Mass spectrometry imaging (MSI) is a particular case in which 2D distribution of analytes can be reconstructed after recording full mass spectra at the coordinate of the "pixels" sampled by a LASER beam. The resolving power and the mass accuracy of analyzers greatly improved to reach values allowing the direct determination of molecular formula of low molecular weight analytes. However, due to the massive amount of information generated now in (ultra) high resolution ((U)HR) MS data,[2] the extraction of chemical information from spectra is becoming more and more challenging.

In 1963, Kendrick[3] introduced a method based on the two-dimensional projection of the atomic composition space enabling a rapid identification of families of compounds. The Kendrick method is based on the transformation of the mass spectra (mass-to charge ratio or m/z in the X-axis and intensity in the Y-axis) to Kendrick plots where the X-axis corresponds to the Kendrick mass (KM) and the Y-axis corresponds to the Kendrick mass defect (KMD). The KM is defined by converting the exact masses of a given group of atoms (the Kendrick base) to the nearest integer value in atomic mass unit (amu). Kendrick's method changes the IUPAC amu reference (i.e., $^{1}/_{12}$ of the ^{12}C mass) to another mass unit (e.g., $^{1}/_{14}$ of the $^{12}C^{1}H_{2}$ radical mass). KM can be calculated from m/z value by the eq 1 where the nominal-$M_{\text{Kendrick reference}}$ and $M_{\text{Kendrick reference}}$ are respectively the nominal mass and the exact mass of the Kendrick reference used for the atomic mass unit definition.

$$\text{KM} = m/z \times \frac{\text{nominal} - M_{\text{Kendrick reference}}}{M_{\text{Kendrick reference}}} \quad (1)$$

The KMD corresponds to the difference between the rounded KM values and the KM (eq 2).

$$\text{KMD} = \text{round}(\text{KM}) - \text{KM} \quad (2)$$

All the compounds differing only by the number of repeating unit of the Kendrick reference will have the same KMD for different KM. Consequently, chemically related compounds will be aligned in the KMD axis on the Kendrick plot, making their identification easier. Recently higher order Kendrick transformations have also been applied when oblique correlations suggest the presence of further repeating units.[4]

Received: July 23, 2019
Accepted: September 11, 2019
Published: September 11, 2019

ACS Publications © 2019 American Chemical Society

DOI: 10.1021/acs.analchem.9b03333
Anal. Chem. 2019, 91, 13112−13118

Over the years, KMD analysis has been extended to the analysis of complex samples composed of chemically related structures, such as petrochemicals, but also polymers or lipids.[5−11]

In this paper, we show that the KMD, which is specific to chemically related homologous series of compounds, can be used to replace the m/z axis of the mean spectra classically used for the analysis of images in MSI. The KMD can be adjusted to filter data in a nontargeted, semitargeted and targeted mode. This approach enables an automated, faster and efficient data processing, allowing the rapid identification and localization of families of compounds in the complex chemical space of the image. This method has been successfully applied to two different types of samples, bacteria cocultures and brain tissue sections.

EXPERIMENTAL SECTION

Materials. The MALDI matrices 2,3-diaminonaphthalene (DAN) and α-cyano-4-hydroxycinnamic acid (HCCA) were purchased from Sigma-Aldrich (Belgium). Acetonitrile and Methanol were LC-MS grade from Biosolve (Belgium). Poly(ethylene oxide) monomethyl ether (CH_3O-PEO-H) having an average nominal mass of 750 g/mol, tetraalkylammonium bromides (reagent grade >98%), trifluoroacetic acid (TFA), formic acid, bovine serum albumin (BSA), methyl-*tert*-butyl ether (MtBE), acetone HPLC grade and sodium chloride were purchased from Sigma-Aldrich (Belgium). Pr. Philippe Jacques (Terra Teaching and Research Center, Microbial Processes and Interactions, University of Liège, Belgium) and Lipofabrik (Lille, France) kindly provided standards of lipopeptides.

Sample Preparation for MALDI-FT-ICR MS Imaging Proof of Concept. DAN matrix solution was prepared at saturation (>30 mg/mL) in ACN/water 70:30 vol/vol spiked with 0.2% TFA. Tetraalkylammonium bromide stock solution was dissolved in ACN to reach the final concentration of 10 μM. Trypsin digestion of BSA using MS grade porcine trypsin (purchased from PIERCE, Thermofisher, Belgium) was prepared at a final concentration of 15 μM in 50% methanol spiked with 0.1% formic acid following the procedure described in the Supporting Information (SI). Lipids were extracted from cultured eukaryotic cells based on Matysah protocol[12] and resuspended in MeOH. Lipopeptides were dissolved in MeOH spiked with 0.1% TFA at final concentration of 10 μM. CH_3O-PEO-H was dissolved in ACN 10 μM NaCl to reach a concentration of 10 μM. Each sample was mixed separately with DAN matrix at a ratio of 1:1, and were spotted randomly on a MALDI AnchorChip target plate (Bruker, Bremen, Germany) in duplicate for high and low resolution MS imaging. In addition, 1 μL of each sample was mixed and DAN matrix was added at a 1:1 ratio and spotted onto the MALDI target plate. Finally, a blank spot of DAN matrix was added.

Bacterial Strains, Medium, and Culture Conditions. The strains used for this study were *Bacillus velezensis* GA1 and *Pseudomonas* sp. CMR12a. Both strains were inoculated on a semisolid agar-based PDA medium (Potato Dextrose Agar) and incubated overnight at 30 °C. At the end of the culture, Petri dishes were sealed with Parafilm M and stored at 4 °C prior to analysis.

Animals, Tissue Sampling, and Sectioning. Mouse brain samples were provided by Prof. Martinez (School of Mental Health and Neuroscience at Maastricht University, Netherlands), and bred in-house as described elsewhere.[13] Animals were sacrificed by CO_2 inhalation and brain tissues were extracted. After extraction, the brains were cut across the sagittal midline and immediately fresh-frozen in liquid nitrogen. The brain parts were subsequently stored at −80 °C. On the day of transport, samples were placed on dry ice and transferred to the University of Liege. All procedures were approved by the Animal Welfare Committee of Maastricht University and were performed according to Dutch federal regulations for animal protection. Frozen brain tissues were sectioned into 14 μm thick sagittal slices using a CryoStar NX70 (Thermo Fisher Scientific, Waltham, MA) at −20 °C and thaw-mounted onto indium−tin oxide (ITO) conductive glass slides (Bruker Daltonics, Bremen, Germany).

Sample Preparation for MALDI-FT-ICR MS Imaging. Microbial colonies on agar and region of interest were cut directly from the Petri dish and transferred to the target ITO plate (Bruker, Bremen, Germany), previously covered with double sided conductive carbon tape (StructureProbe INC, West Chester, PA). This assembly was then placed in a vacuum desiccator until complete drying (overnight). A HCCA matrix solution was prepared at the concentration of 5 mg/mL in ACN/water 70:30 vol/vol spiked with 0.2% TFA, based on the previous work of Debois et al.[14] Application of the matrix solution on the dried bacterial sample was performed using the SunCollect (SunChrom, Friedrichsdorf, Germany) spraying system. In total, 60 layers of HCCA matrix were sprayed on the sample. The first three layers were sprayed at 5 μL/min, and the other at 10 μL/min. Mouse brain tissue slides deposed on ITO slides were first put into a vacuum desiccator for approximatively 20 min. A solution of HCCA at the concentration of 5 mg/mL in MeOH/water 90:10 vol/vol spiked with 0.2% TFA was prepared, and sprayed onto the dried sample by the SunCollect. The number of spraying layers were set to 30, at a spraying speed of 10 μL/min, except for the three first layers sprayed at 5 μL/min.

FT-ICR Mass Spectrometry. Mass spectrometry images were obtained using a FT-ICR mass spectrometer (SolariX XR 9.4T, Bruker Daltonics, Bremen, Germany). The mass spectrometer was systematically mass calibrated from 200 m/z to 2,300 m/z before each analysis with a red phosphorus solution in pure acetone spotted directly onto the ITO Glass slide or onto the MALDI plate to reach a mass accuracy better than 0.5 ppm. FlexImaging 5.0 (Bruker Daltonics, Bremen, Germany) software was used for MALDI MS imaging acquisition, with a pixel step size for the surface raster set to 150 μm for Kendrick proof of concept imaging and to 100 μm for bacteria and brain tissue imaging. For each mass spectrum, one scan of 20 LASER shots was performed at a repetition rate of 200 Hz. The LASER power was set to 50% and the beam focus was set to "small". The mass spectra for high and low resolution mass images were recorded by setting the number of data points in the transient at respectively 1 000 000 (1M) and 256 000 (256 K).

Kendrick Filtering for Data Reduction and Clustering. MSconvert (Proteowizard)[15] and Fleximaging 5.0 (Bruker) have been respectively used to convert MS raw files (obtained from, for example, direct infusion MS, liquid chromatograph MS, ion mobility MS···) to mzML and MSI raw files (obtained from imaging MS) to imzML files. These files are processed under Python in-house software (MSKendrickFilter, available upon request from c.kune@uliege.be).

DOI: 10.1021/acs.analchem.9b03333
Anal. Chem. 2019, 91, 13112−13118

After a conversion to binary format files (.ICK), specifically designed for our software, data are filtered based on the KMD. For a MS analysis, the .ICK file contains the mass-to-charge and intensity information for each detected ion of each recorded scan (or pixel in case of MSI application). A noise reduction, based on a minimum intensity threshold, can be applied to limit the.ICK file size and the CPU and RAM usage of the software.

The Kendrick filtering method workflow for MSI data or MS data (e.g., direct infusion, chromatogram, mobilogram, electrophoregram···) is depicted in Figure 1. Once the .ICK file has been generated, an ion list containing all the m/z present in the mean spectrum (sum of each MS spectra in MS or MSI data) is created. The software calculates a Kendrick mass defect (KMD) for each m/z value according to eq 1 and eq 2 in the user-defined Kendrick reference (i.e., $-CH_2-$ in this work). Different rounding functions are available in our software, that is, floor, ceil, and round. Floor option has been used for the results reported here. All m/z ratio are then associated with a KMD. The second step consists in filtering the total ion list by keeping only the ions whose KMD is included in the user-defined KMD range. A m/z ratio selection range can also be applied as a criterion for data filtering. The resulting ion list contains chemically related compounds. In the case of different compound families sharing a similar KMD, an additional algorithm is added to cluster the saved ion by compound families. This clustering step (reported as mass difference clustering algorithm in Figure 1) groups ions according to their mass difference corresponding to a multiple of the chosen Kendrick reference mass. The software allows a user-defined m/z tolerance value (e.g., here we used 5 and 2 ppm for m/z tolerances with resolution of, 20 000 and 160 000 full width at half-maximum, fwhm, at 410 m/z, respectively). In this version of the software, isotope compounds are considered as different families due to Kendrick mass defect deviations. This algorithm generates an ion list for each putative compound family. Finally, a chromatogram (for liquid chromatography or gas chromatography MS), a mobilogram (for ion mobility MS), an electrophoregram (for capillary electrophoresis MS) or an image (for MSI) can be generated from these ion lists. The entire process can be repeated with different KMD and m/z ranges to generate additional MS data of different compound families.

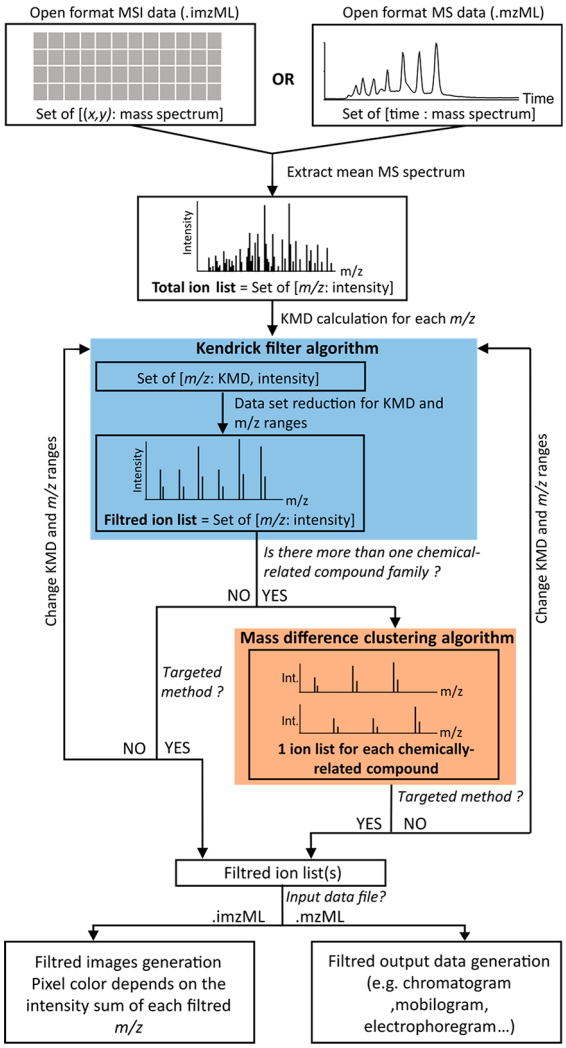

Figure 1. Kendrick filtering method workflow applied on MSI data and MS data (such as chromatography, ion mobility, capillary electrophoresis···).

In this work, we only focused the Kendrick filtering application on MSI data as a rapid visualization and localization tool of chemically related compounds. An intensity threshold value of 200.000 counts per scan and a normalization to the total ion current (TIC) for each pixel was applied for all the reported images.

RESULTS AND DISCUSSION

KMD Filtering Concept Applied to MS Data. The illustration of the KMD filtering concept is shown in Figure 2 for a MALDI FT-ICR MS data. The MALDI spots were prepared with a mix of different compound families including lipids, lipopeptide, polymers, tetraalkylammonium (TAA) and peptides of BSA tryptic digest. The resulting mass spectra (Figure 2B) is rather complex and the assignment of MS peak associated with compounds families is challenging. The Kendrick plot (Figure 2A), generated using $-CH_2-$ as Kendrick reference significantly reduces the complexity by aligning the compounds bearing a repeating unit of $-CH_2-$. Tetraalkylammonium, lipids, and lipopeptides families are then easily detected (respectively highlighted in blue, green, and orange), and can be quickly selected in a rectangular area in the KMD plot. Polymers families, which are in the same mass range of lipids families, are revealed by changing the Kendrick reference to the repeating monomer unit $-C_2H_4O-$ (see SI Figure S1). Thus, the goal of the proposed Kendrick filtering method relies on its capacity to extract the relevant peaks associated with a given family of compounds from a raw mass spectrum and to generate a new filtered spectrum, chromatogram, mobilogram, or image. Depending on the mass spectrometer resolution, setting a KMD range as well as a MS range might not be sufficient to isolate a single family of chemically related compounds. Indeed, it can be explained by the presence of other compounds exhibiting similar KMD and m/z. In these cases, the mass difference clustering algorithm (see the Materials section) can be applied to separate overlapping families of compounds. Thus, a sequential strategy consisting in first filtering by KMD and then by the mass difference clustering gives clean filtered spectra of tetraalkylammonium (Figure 2.C), surfactins (lipopeptides family, Figure 2.D) and phosphatidylcholines (lipid family, Figure 2.E) from a MALDI spot.

DOI: 10.1021/acs.analchem.9b03333
Anal. Chem. 2019, 91, 13112−13118

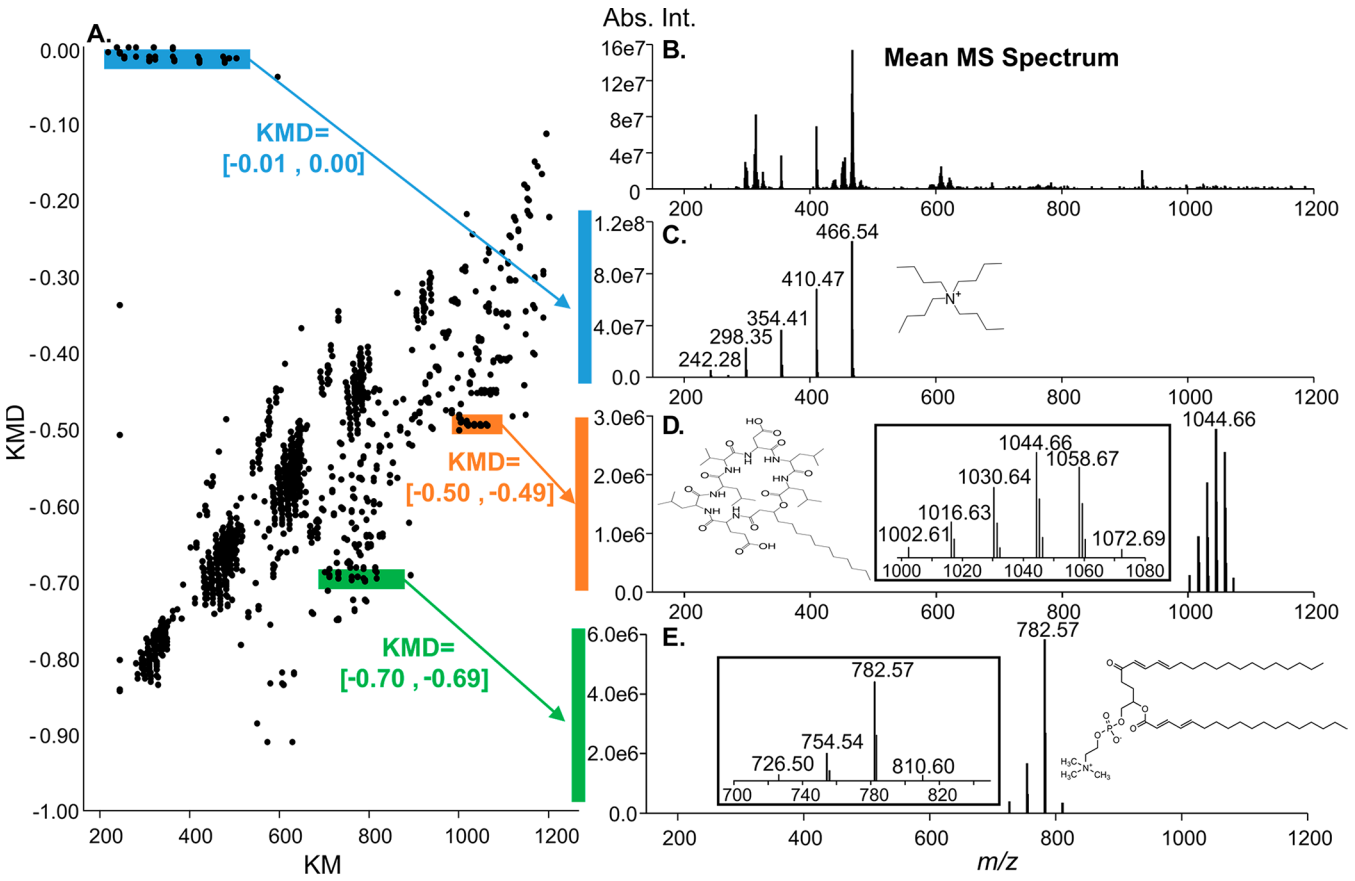

Figure 2. Illustration of the KMD filtering method. (A) Kendrick mass defect plot of the spectra obtained by FT-ICR MS. (B) Full MS spectrum when no filtration is applied. By selecting a specific KMD range and eventually a specific mass range, it is possible to filter the MS Spectra and show only the chemically related molecules such as TAA (C), lipopeptides: surfactins (D) or lipids: phosphatidylcholines (E).

KMD Filtering Concept Applied to MSI Data. As a proof-of-concept, but also to assess the effectiveness of KMD filtering process on MSI data, we randomly spotted a MALDI AnchorChip plate with several droplets of lipids, tetraalkylammonium salts, lipopeptides and polymers (Figure 3.A). The proposed KMD filtering algorithm developed here was applied on the imaging data set, using directly the KMD values previously obtained in the MS analysis. The MSI data were acquired with two different MS resolution calculated at the *m/z* 410 (i.e., 20 000 and 160 000, respectively). A mixture spot (spot 8, containing all the investigated compound families) and a blank matrix spot (Spot 3) were added as a positive and a negative control, respectively.

Lipids, lipopeptides and TAA were isolated using the $-CH_2-$ reference, polymers were isolated using the $-C_2H_4O-$ reference (see SI Figure S2). The KMD filtering process allowed to determine the precise localization of each chemically related compounds for both MS resolution acquired data sets. The similarities of the images produced at 20 K and 160 K resolution is in fact ensured by the mass difference clustering algorithm. In addition, one should note that none of the targeted compounds were found in the negative control spot 3 at both selected MS resolution.

These results outline the power of KMD filtering approach as a rapid visualization tool on MSI data generated from (U)HR MS analyzer with different MS resolutions.

MALDI Imaging of Bacterial Culture. Mass spectrometry imaging of bacterial culture has gained growing attention.[14,16−19] By combining the chemical identification of a compound with its localization, MSI could notably provide more insights into the bacterial interspecies molecular interactions. The objective would be to detect and localize compounds of interest, such as lipopeptides, produced by the bacteria in different environments or at different incubation times. Since most of lipopeptides contain a variable hydrophobic lipid chain-length,[20] applying a KMD plot with a $-CH_2-$ repeating unit, seems to be a fit-for-purpose approach to rapidly screen the detected compounds in the region of interest. The results were analyzed according to a nontargeted approach, by screening along the KMD axis different families of compounds (Figure 4). These compounds were then identified based on their exact mass. Three different families of lipopeptides were detected and identified as iturins (Figure 4B), surfactins (Figure 4C) and sessilins (Figure 4F). As expected, the distribution of lipopeptides differs according to the different families. Surfactins and iturins are secreted by *Bacillus* and readily diffuse in the agar medium, suggesting an interplay between *Bacillus* and *Pseuomonas*.[21] By contrast, the sessilins formed by *Pseudomonas*, remained associated with the cells and are not detected outside the bacterial colony.

In the KMD range −0.65 to −0.66, at least two different lipid families were detected (Figure 4D and E). Thanks to the mass difference clustering algorithm, it is possible to discriminate these two groups. The first group of lipids (Figure 4.D) contained the *m/z* values: 710.444, 724.459, and 738.477, belonging to the sub class 1-(1Z-alkenyl)2-acylglycerophosphoethanolamines of the glycerophosphoethanolamines lipid class. Based on its localization on the ITO slide, this lipid

DOI: 10.1021/acs.analchem.9b03333
Anal. Chem. 2019, 91, 13112−13118

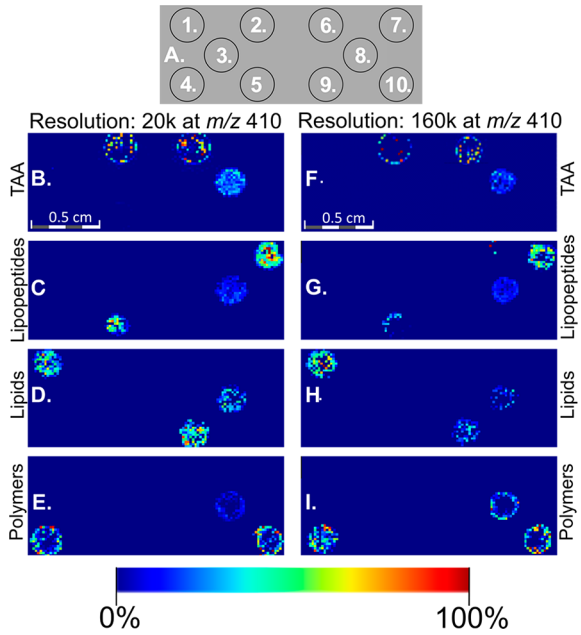

Figure 3. KMD filtering applied on MALDI mass spectrometry imaging data where different chemically related compounds were randomly spotted on a MALDI AnchorChip target plate. A. Scheme of the distribution of chemically related compounds (spots 1. and 9.: lipids, spots 2. and 6.: tetraalkylammonium, spot 3.: matrix, spot 4. and 10.: polymers, spots 5. and 7.: lipopeptides, spot 8.: Mix). B to E are generated image after KMD filtering for, respectively, TAA, lipopeptides, lipids and polymers from MSI data with a MS resolution of fwhm 20 000 for m/z 410. F to I are generated image after KMD filtering for, respectively, TAA, lipopeptides, lipids and polymers from MSI data with a MS resolution of fwhm 160 000 for m/z 410. The color scale represents a normalized intensity of the ions.

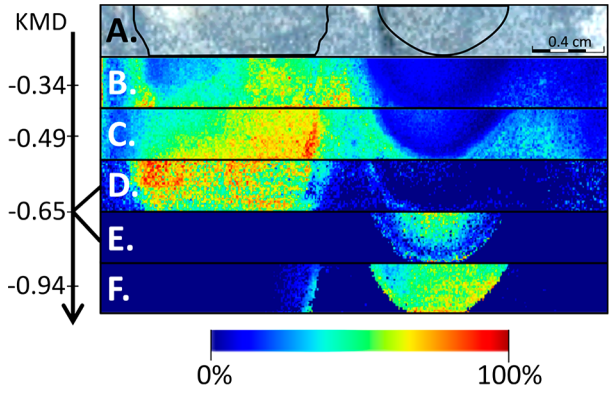

Figure 4. KMD filtering applied on MALDI Imaging of bacterial culture. (A) Optical image of the sample covered with matrix, *Bacillus* is circled on the left side, and *Pseudomonas* is circled on the right side. The identified families are presented according to their KMD value. (B) Iturins A (sodium adducts) at the KMD range −0.33 to −0.35 (C) Surfactins (sodium adducts) at the KMD range −0.49 to −0.51. (D) and (E) identification of two different lipid classes at the KMD range −0.65 to −0.66, (F) Sessilins (sodium adducts) at the KMD range −0.93 to −0.95. The color scale represents the normalized intensity of the ions.

group was specifically related to *Bacillus velezensis* GA1. The second group of lipids (Figure 4.E) composed of the following m/z values; 734.472 and 748.487 was identified as diacylglycerophosphoethanolamines or diacylglycerophosphocholines. Their spatial distribution was specific to *Pseudomonas* sp. CMR12a.

MALDI Imaging of a Mouse Brain Section. The last example treated in this paper belongs to MSI applied on mice tissue. MSI enables the localization of a set of diverse molecules in a specific tissue, such as brain,[22] liver,[23] or kidney,[24] providing local molecular information for a better understanding of illnesses and deeper insights into physiological mechanisms. Among the detected compounds, lipids represent a high percentage of ions since they are present in every cell by constituting the membranes and energy storage vesicles.[25,26] Their implication in various biological functions and their capacity to reflect the physiological and environmental conditions makes their study essential for understanding diseases or biomarker discovery.[27−30] The results obtained by MSI of a mouse brain section (Figure 5) shows

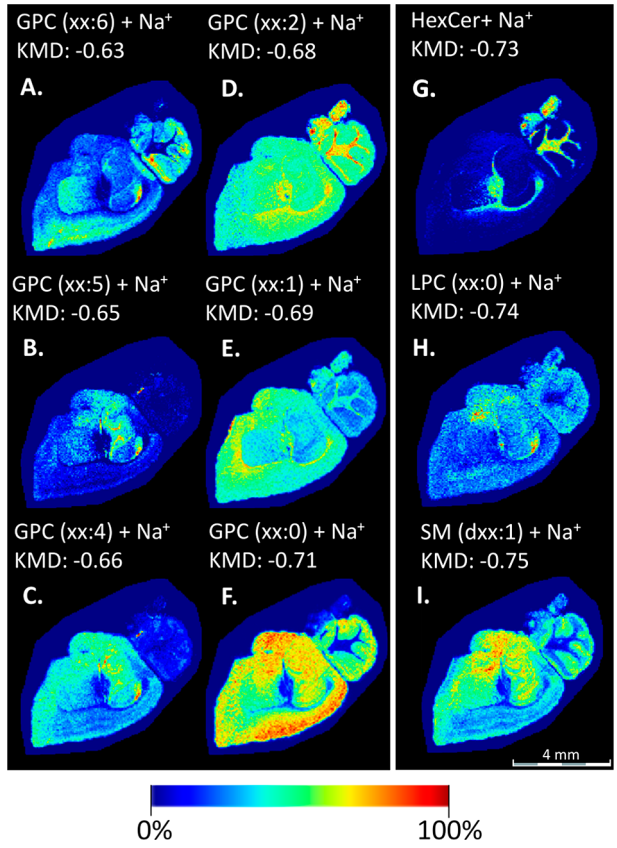

Figure 5. KMD filtering applied on MALDI imaging of a sagittal slice of mouse brain. (A) to (F) Image of sodiated glycerophosphocholines,$[GPCs+Na]^+$ with 6, 5, 4, 2, 1, and 0 insaturations, respectively. (G) Image of sodiated hexosylceramides, $[HexCers+Na]^+$. (H) Image of sodiated lysophoshocholins, $[LPCs+Na]^+$. (I) Image of sodiated sphingomyelins, $[SMs+Na]^+$. The color scale represents the normalized intensity of the ions.

different patterns of lipid distribution belonging to the families of glycerophosphocholines (GPCs), hexosylceramides (HexCers), lysophoshocholins (LPCs), and sphingomyelins (SMs) classes, as described in the literature on brain tissue analysis.[31,32] The software shows the list of peaks used to build the distribution of each family. From that list, individual distributions can be obtained. All the detected families of compounds were tentatively assigned according to their class (GPCs, SMs, LPCs) and according to their unsaturation

DOI: 10.1021/acs.analchem.9b03333
Anal. Chem. 2019, 91, 13112−13118

(xx:n), where "xx" represents the number of carbon and "n" corresponds to the number of unsaturation. The attribution of a specific class was done based on high-resolution MS data, using LIPIDMAPS database (The LIPID MAPS Lipidomics Gateway, http://www.lipidmaps.org/). The database search was performed only on even-chain lipids, with a mass tolerance of ±0.005 m/z. The list of detected compounds and tentatively assigned compounds is available in SI Figure S3. An additional image on an adjacent section of the mouse brain tissue was recorded in the same experimental conditions to confirm the reproducibility of the spatial distribution after KMD filtering (see SI Figure S4). Brain regions (see SI Figure S5) were identified according to the Allen mouse brain atlas (https://mouse.brain-map.org/).

Interestingly, after applying our Kendrick filtering software, some of the detected GPCs from mouse brain tissue sections tend to be differentially colocalized, depending on their unsaturation degree. At six unsaturations on the lipid chain (Figure 5A. and SI Figure S6), GPCs are mainly detected in the isocortex, the cerebral nuclei and cerebellar cortex, while GPCs with 5 unsaturations are detected mainly in the hippocampal formation (Figure 5B. and SI Figure S6), and the GPCs with four unsaturations are detected in the hippocampal formation and the olfactory areas (Figure 5C). When the GPCs lipid chain contains one or two unsaturations, they are mainly localized in the fiber tracts (Figure 5D and E.), but when the GPCs are fully unsaturated (Figure 5F), they will be detected only in the cerebrum and cerebellar cortex. This variation in the localization of GPCs conforms to previous imaging data of lipids in brain tissue.[33] Finally, additional relevant lipid distribution can also be detected, such as the specific localization of HexCers in the fiber tracts (Figure 5G.), of LPCs mainly in the hippocampal formation (Figure 5H.), and the SMs in the hippocampal formation, the cerebral nuclei, the olfactory area and the cerebellar cortex (Figure 5I.).

By applying the KMD MSI data filtering approach proposed here, any type of biological modification occurring on lipids such as shorter or longer lipid chain length or lipid oxidation could be easily detected on the KMD plot. Image reconstruction based on the KMD plot provides, for a given KMD range, a specific lipid fingerprint that can further be used to compare different images.

CONCLUSION

In this work, we have used KMD as a filtering tool to visualize the chemically related compounds in complex mass spectra, as described in the literature. The mass resolving power and mass accuracy of modern instruments ensure an accurate KMD filtering. For overlapping families, a second filtering process using the mass distance between peaks has been introduced. Based on those selection criteria, we were able to group compounds presenting the same KMD in a single spectrum and to apply the KMD analysis to molecular images obtained by MALDI MSI where it reveals all its power. Replacing the m/z axis of the reconstructed mean mass spectrum by a KMD axis brings a real benefit for rapid and automatic image reconstruction not only for specific organic molecules but also for families, speeding up the identification process and facilitating data analysis. The use of the KMD over normal mass[34] defect enables to choose the reference unit adapted ($-CH_2-$ for lipids, $-C_2H_4O-$ for polymers), and simplifies the area selection on the KMD plot, since all the chemically related families would be aligned. Finally, future developments on higher-order KMD will be soon implemented in our software. The developed approach has been successfully applied through two practical examples, that is, bacterial cocultures and histological sections of mouse brain. The KMD filtering method applied to bacterial culture image data has permitted the rapid detection and localization of different groups of compounds, such as lipopeptides or lipids. The application of the KMD filtering method to histological tissue sections of a mouse brain highlighted the localization of lipids according to their family and their number of unsaturation.

In light of these results, we argue that the methodology outlined in this paper can be used as a nontargeted screening tool, reconstructing the image by scanning the KMD scale according to the workflow proposed in Figure 1. Nontargeted, semi targeted or targeted modes are different options developed in the software, allowing to rapidly detect and localize metabolites containing the repetitive unit of the substrate molecule or a specific family of compounds, through their known KMD. The same approach can be extended to any type of data sets in mass spectrometry imaging with different ionization process (e.g., MALDI MSI or DESI MSI) but also when MS is hyphenated with separation methods, no matter the separation method employed (e.g., ion mobility or liquid chromatography) or the mass analyzers used.

ASSOCIATED CONTENT

Supporting Information

The Supporting Information is available free of charge on the ACS Publications website at DOI: 10.1021/acs.analchem.9b03333.

Full detailed experimental section, KMD analysis applied on polymers (S1), KMD plots for KMD filtering applied on MALDI mass spectrometry imaging data (S2), List of identified compounds after KMD filtering applied on MALDI imaging of a sagittal mouse brain (S3), KMD filtering applied on MALDI imaging of a sagittal slice of mouse brain tissue (S4), annotated sagittal mouse brain slice (S5). and individual lipid distribution on sagittal slice of mouse brain tissue (S6) (PDF)

AUTHOR INFORMATION

Corresponding Author

*E-mail: e.depauw@uliege.be.

ORCID

Christopher Kune: 0000-0002-3010-8173
Andréa McCann: 0000-0002-1093-6414
Loïc Quinton: 0000-0001-8153-9590
Edwin De Pauw: 0000-0003-3475-1315

Author Contributions

‖C.K. and A.M. contributed equally.

Notes

The authors declare no competing financial interest.

ACKNOWLEDGMENTS

We thank Prof. Philippe Jacques, from the Microbial Processes and Interactions (MiPI) research unit of Gembloux Agro-Bio Tech (Belgium) and Lipofabrik (Lille, France) for providing lipopeptides samples. We acknowledge financial support from the Excellence Of Science Program of the FNRS F.R.S (Rhizoclip EOS 18000802), from the Interreg EMR project: EURLIPIDS (R-8598) and from the European Union's

DOI: 10.1021/acs.analchem.9b03333
Anal. Chem. 2019, 91, 13112−13118

Horizon 2020 research and innovation program under grant agreement No. 731077. Finally, we acknowledge the European Union and Wallonia program FEDER for the founding of the instruments (SolariX XR 9.4T). All experiments were done with permission from the Committee on Animal Welfare of Maastricht University, according to Dutch governmental rules.

REFERENCES

(1) Schmitt-Kopplin, P.; Hertkorn, N. *Anal. Bioanal. Chem.* **2007**, *389* (5), 1309−1310.
(2) Cho, Y.; Ahmed, A.; Islam, A.; Kim, S. *Mass Spectrom. Rev.* **2015**, *34* (2), 248−263.
(3) Kendrick, E. *Anal. Chem.* **1963**, *35* (13), 2146−2154.
(4) Roach, P. J.; Laskin, J.; Laskin, A. *Anal. Chem.* **2011**, *83* (12), 4924−4929.
(5) Hughey, C. A.; Hendrickson, C. L.; Rodgers, R. P.; Marshall, A. G.; Qian, K. *Anal. Chem.* **2001**, *73* (19), 4676−4681.
(6) Marshall, A. G.; Rodgers, R. P. *Acc. Chem. Res.* **2004**, *37* (1), 53−59.
(7) Morgan, T. E.; Ellacott, S. H.; Wootton, C. A.; Barrow, M. P.; Bristow, A. W. T.; Perrier, S.; O'Connor, P. B. *Anal. Chem.* **2018**, *90* (19), 11710−11715.
(8) Lerno, L. A.; German, J. B.; Lebrilla, C. B. *Anal. Chem.* **2010**, *82* (10), 4236−4245.
(9) Nakamura, S.; Cody, R. B.; Sato, H.; Fouquet, T. *Anal. Chem.* **2019**, *91* (3), 2004−2012.
(10) Zheng, Q.; Morimoto, M.; Sato, H.; Fouquet, T. *Fuel* **2019**, *235*, 944−953.
(11) Roullier-Gall, C.; Witting, M.; Gougeon, R. D.; Schmitt-Kopplin, P. *Front. Chem.* **2014**, *2*, 102.
(12) Matyash, V.; Liebisch, G.; Kurzchalia, T. V.; Shevchenko, A.; Schwudke, D. *J. Lipid Res.* **2008**, *49* (5), 1137−46.
(13) Youmans, K. L.; Tai, L. M.; Nwabuisi-Heath, E.; Jungbauer, L.; Kanekiyo, T.; Gan, M.; Kim, J.; Eimer, W. A.; Estus, S.; Rebeck, G. W.; Weeber, E. J.; Bu, G.; Yu, C.; Ladu, M. J. *J. Biol. Chem.* **2012**, *287* (50), 41774−86.
(14) Debois, D.; Ongena, M.; Cawoy, H.; De Pauw, E. *J. Am. Soc. Mass Spectrom.* **2013**, *24* (8), 1202−13.
(15) Chambers, M. C.; Maclean, B.; Burke, R.; Amodei, D.; Ruderman, D. L.; Neumann, S.; Gatto, L.; Fischer, B.; Pratt, B.; Egertson, J.; Hoff, K.; Kessner, D.; Tasman, N.; Shulman, N.; Frewen, B.; Baker, T. A.; Brusniak, M. Y.; Paulse, C.; Creasy, D.; Flashner, L.; Kani, K.; Moulding, C.; Seymour, S. L.; Nuwaysir, L. M.; Lefebvre, B.; Kuhlmann, F.; Roark, J.; Rainer, P.; Detlev, S.; Hemenway, T.; Huhmer, A.; Langridge, J.; Connolly, B.; Chadick, T.; Holly, K.; Eckels, J.; Deutsch, E. W.; Moritz, R. L.; Katz, J. E.; Agus, D. B.; MacCoss, M.; Tabb, D. L.; Mallick, P. *Nat. Biotechnol.* **2012**, *30* (10), 918−20.
(16) Yang, J. Y.; Phelan, V. V.; Simkovsky, R.; Watrous, J. D.; Trial, R. M.; Fleming, T. C.; Wenter, R.; Moore, B. S.; Golden, S. S.; Pogliano, K.; Dorrestein, P. C. *J. Bacteriol.* **2012**, *194* (22), 6023−6028.
(17) Debois, D.; Jourdan, E.; Smargiasso, N.; Thonart, P.; De Pauw, E.; Ongena, M. *Anal. Chem.* **2014**, *86* (9), 4431−4438.
(18) Boya, P. C. A.; Fernández-Marín, H.; Mejía, L. C.; Spadafora, C.; Dorrestein, P. C.; Gutiérrez, M. *Sci. Rep.* **2017**, *7* (1), 5604.
(19) Dunham, S. J. B.; Ellis, J. F.; Li, B.; Sweedler, J. V. *Acc. Chem. Res.* **2017**, *50* (1), 96−104.
(20) Ongena, M.; Jacques, P. *Trends Microbiol.* **2008**, *16* (3), 115−125.
(21) Molina-Santiago, C.; Pearson, J. R.; Navarro, Y.; Berlanga-Clavero, M. V.; Caraballo-Rodriguez, A. M.; Petras, D.; Garcia-Martin, M. L.; Lamon, G.; Haberstein, B.; Cazorla, F. M.; de Vicente, A.; Loquet, A.; Dorrestein, P. C.; Romero, D. *Nat. Commun.* **2019**, *10* (1), 1919.
(22) Stoeckli, M.; Staab, D.; Staufenbiel, M.; Wiederhold, K.-H.; Signor, L. *Anal. Biochem.* **2002**, *311* (1), 33−39.
(23) Shimma, S.; Sugiura, Y.; Hayasaka, T.; Hoshikawa, Y.; Noda, T.; Setou, M. *J. Chromatogr. B: Anal. Technol. Biomed. Life Sci.* **2007**, *855* (1), 98−103.
(24) Zoriy, M.; Matusch, A.; Spruss, T.; Becker, J. S. *Int. J. Mass Spectrom.* **2007**, *260* (2), 102−106.
(25) Murphy, R. C.; Hankin, J. A.; Barkley, R. M. *J. Lipid Res.* **2009**, *50* (Suppl), S317−22.
(26) Burnum, K. E.; Cornett, D. S.; Puolitaival, S. M.; Milne, S. B.; Myers, D. S.; Tranguch, S.; Brown, H. A.; Dey, S. K.; Caprioli, R. M. *J. Lipid Res.* **2009**, *50* (11), 2290−2298.
(27) Wenk, M. R. *Nat. Rev. Drug Discovery* **2005**, *4* (7), 594−610.
(28) Orešič, M.; Hänninen, V. A.; Vidal-Puig, A. *Trends Biotechnol.* **2008**, *26* (12), 647−652.
(29) Yang, K.; Han, X. *Trends Biochem. Sci.* **2016**, *41* (11), 954−969.
(30) Lam, S. M.; Shui, G. *J. Genet. Genomics* **2013**, *40* (8), 375−390.
(31) Sparvero, L. J.; Amoscato, A. A.; Dixon, C. E.; Long, J. B.; Kochanek, P. M.; Pitt, B. R.; Bayır, H.; Kagan, V. E. *Chem. Phys. Lipids* **2012**, *165* (5), 545−562.
(32) Ellis, S. R.; Paine, M. R. L.; Eijkel, G. B.; Pauling, J. K.; Husen, P.; Jervelund, M. W.; Hermansson, M.; Ejsing, C. S.; Heeren, R. M. A. *Nat. Methods* **2018**, *15* (7), 515−518.
(33) Carter, C. L.; McLeod, C. W.; Bunch, J. *J. Am. Soc. Mass Spectrom.* **2011**, *22* (11), 1991.
(34) McDonnell, L. A.; van Remoortere, A.; de Velde, N.; van Zeijl, R. J. M.; Deeldera, A. M. *J. Am. Soc. Mass Spectrom.* **2010**, *21* (12), 1969−1978.

DOI: 10.1021/acs.analchem.9b03333
Anal. Chem. 2019, 91, 13112−13118